3D printing of an *in situ* grown MOF hydrogel with tunable mechanical properties

Wangqu Liu¹, Ozan Erol², David H. Gracias^{1,3,4*}

*Corresponding author: dgracias@jhu.edu

Keywords: metal-organic frameworks, composites, stretchable hydrogel, wearables, flexible sensors, adsorption

¹ Department of Chemical & Biomolecular Engineering Johns Hopkins University, 3400 North Charles Street, Baltimore, MD 21218, USA

² Department of Mechanical Engineering and Hopkins Extreme Materials Institute Johns Hopkins University, 3400 North Charles Street, Baltimore, MD 21218, USA

³ Department of Materials Science and Engineering Johns Hopkins University, 3400 North Charles Street, Baltimore, MD 21218, USA

⁴ Department of Chemistry Johns Hopkins University, 3400 North Charles Street, Baltimore, MD 21218, USA

Abstract

Due to their precisely modifiable microporosity and chemical functionality, metal-organic frameworks (MOFs) have revolutionized catalysis, separations, gas storage, drug delivery, and sensors. However, because of their rigid and brittle powder morphology, it is challenging to build customizable MOF shapes with tunable mechanical properties. Here, we describe a new 3D printing approach to create stretchable and tough MOF hydrogel structures with tunable mechanical properties. We formulate a printable ink by combining prepolymers of a versatile double network (DN) hydrogel of acrylamide and alginate, a shear thinning agent, and MOF ligands. Importantly, by simultaneous crosslinking of alginate and in situ growth of the HKUST-1 using copper ions, we are able to create composites with high MOF dispersity in the DN hydrogel matrix with high pore accessibility. We extensively characterize the inks and uncover parameters to tune modulus, strength and toughness of the 3D prints. We also demonstrate excellent performance of the MOF hydrogels for dye absorption. Our approach incorporates all the advantageous attributes of 3D printing while offering a rational approach to merge stretchable hydrogels and MOFs and our findings are of broad relevance to wearables, implantable and flexible sensors, chemical separations and soft robotics.

INTRODUCTION

Metal-organic frameworks (MOFs) or crystalline nanoporous materials with metal ions or clusters connected by organic ligand linkers are well-known for their extremely high internal surface area and ordered periodic porosity. Synthetic tunability of the constituent metal ions and organic ligands in MOFs can enable versatile chemical and physical properties. ^{1–3} MOFs have been widely used in separations, ^{4,5} gas storage, ⁶ drug delivery, ^{7,8} catalysis, ⁹ and sensors. ^{10,11} Despite the impressive properties of MOFs demonstrated in laboratory-scale applications, many MOFs are rigid and brittle, and difficult to shape due to their powder form which limits their use in many real-world applications. ^{12,13} Consequently, an important research focus is the development of methods to create composites and processing methods to shape MOFs with other materials such as polymers and ceramics. ¹⁴

Flexible MOF composites that incorporate polymer matrices are deformable and have been used to create wearables, ¹⁵ implantable sensors, ¹⁶ self-folding actuators, ¹⁷ supercapacitors, ^{18,19} and in applications requiring large deformation or resistance to deformation. ^{20,21} However, conventional fabrication methods for MOF-polymer composites such as molding, electrospinning, and surface coating have limited shape complexity and have been used to define primarily simple shapes such as films, ^{4,5} filaments, ^{22,23} and microspheres. ²⁴

3D printing is a fabrication paradigm that offers significant advantages including compact, portable and unskilled manufacturing with complexity, variety, customization, and broad design space.²⁵ In recent years, several researchers have demonstrated 3D printing of MOF-polymer composites via direct ink writing (DIW), digital light processing (DLP) and fused deposition modeling (FDM) for applications in water treatment,^{26–28} gas storage,^{29,30} drug release,³¹ and energy storage.³² However, most of the previously 3D printed MOF-polymer composites used

relatively rigid and brittle matrices such as acrylonitrile butadiene (ABS) and polyvinyl alcohol (PVA) monoliths. Apart from lacking flexibility, the existing 3D printing MOF-polymer composites have critical limitations such as poor porosity and low MOF loading efficiency. Specifically, the most common method to 3D print MOF-polymer composites is by directly blending MOF particles into a polymer solution and 3D printing the mixture. Direct blending often results in particle aggregation and poor particle matrix junction.^{23,33} Also, the non-porous matrix materials often used in these blends can reduce the effective MOF porosity,³⁴ thereby limiting performance. To overcome this problem, *in situ* growth of MOFs have been investigated, but most studies grow MOFs primarily on the surface and not in the bulk of the printed scaffold,^{26,27} resulting in low effective MOF loading and inhomogeneous composites.

Herein, we demonstrate 3D printing of a highly stretchable *in situ* grown MOF-hydrogel composite with several key advances. First, we introduce the concept of 3D printing of a double network (DN) hydrogel precursor with MOF ligands, followed by UV curing, *in situ* MOF growth, and ionic cross-linking to create customizable 3D MOF hydrogel shapes. Unlike prior *in situ* growth demonstrations which featured primarily surface loaded MOF shapes, our approach enables relatively uniformly loaded 3D printed MOF shapes. This facile synthesis method works in aqueous solution at room temperature, doesn't require complicated heating profiles, mechanical stirring, or microwave processing as is needed in conventional MOFs synthesis.³ Second, we formulate a new ink which composed of several components including prepolymers for a double network hydrogel, crosslinker, ultraviolet (UV) initiator, MOF ligand, deprotonating and shear thinning agent. We uncover optimal formulation as well as 3D printing and post-processing parameters for fabricating a HKUST-1 prototypical MOF hydrogel, by careful optimization for ink rheological properties, printing, and processing conditions. Finally, we extensively

characterize the 3D printed HKUST-1 hydrogel composites and observe relatively uniform distribution of MOF particles in DN hydrogel matrix with high dispersity and excellent MOF performance in dye absorption measurements. Also, by using a DN hydrogel, 3D printed shapes are stretchable and tough, and their mechanical properties can be tuned. The printed structures are stretchable up to approximately 453.0 % and their moduli and toughness can be varied to as high as 152.3 kPa and 744.7 kJ/m⁻³. Our study provides a versatile and rational platform for efficient 3D printing of flexible MOF-polymer composites of broad relevance.

RESULTS AND DISCUSSIONS

Formulation of hydrogel precursor ink and fabrication of MOF hydrogel

The composition of our hydrogel precursor ink consists of four main components (Fig. 1A). The first component (color coded red in Fig. 1A) contains the monomer acrylamide (AAm), the crosslinker *N*, *N*'-methylenebisacrylamide (MBAA), and the ultraviolet photoinitiator Irgacure 2959 (12959) which are needed to form the primary polymer network. The second component (color coded dark blue in Fig. 1A) consists of sodium alginate (SA) which is needed to form the secondary polymer network in a double network hydrogel. The third component (color coded light blue in Fig. 1A) consists of trimesic acid (H₃BTC) as the organic ligand and triethylamine (TEA) as the deprotonating agent for the HKUST-1 MOF synthesis. Finally, the fourth component (color coded green in Fig. 1A) is hydroxyethylcellulose (HEC) which functions as the shear-thinning agent needed for 3D printing. The pAAm/alginate DN hydrogel was chosen as the flexible matrix because previous literature has shown it to form highly stretchable and tough hydrogels, and the mechanical performance of the hydrogel system can be readily tuned the by changing the amount of monomer and crosslinking density.³⁵ We chose to synthesize an HKUST-1 (also known as Cu-

BTC, [Cu₃(BTC)₂, BTC = 1,3,5-benzenetricarboxylate]) composite because HKUST-1 is a good prototypical MOF that is readily synthesized with presence of Lewis base under mild conditions. A key challenge in formulating an ink for DIW printing is that the 3D printing ink must have shear-thinning properties, like toothpaste. The most common way to achieve this property is to add a shear-thinning agent. However, most of the commercial available shear-thinning agents for DIW 3D printing ink such as Laponite nanoclay,^{36,37} or gellan gum³⁸ are ionic shear-thinning agents that interact via electrostatic forces that are screened by the ions in the presence of HKUST-1 MOF components H₃BTC and TEA. Hence, it was necessary to use a non-ionic molecule HEC (Natrosol) to induce the shear-thinning property in our hydrogel precursor ink.³⁹

The overall fabrication for the 3D printed HKUST-1 hydrogel structures is schematically illustrated in Figure 1B. We first loaded the hydrogel MOF precursor mixture into a cartridge and 3D printed a previously designed shape. Then, we photocured the printed structure using a homebuilt UV (wavelength 365 nm) curing system. Upon exposure to UV light, the initiator 12959 is excited and initiates free-radical polymerization of the primary pAAm network. The pAAm and alginate polymer networks are intertwined and joined by covalent crosslinking between the amine groups on the polyacrylamide chains and the carboxyl groups on the alginate chains (represented by red squares and blue triangles in Fig. 1A, respectively). Then, we immersed the UV cured hydrogel matrix print into a Cu(NO₃)₂ solution to facilitate simultaneous alginate crosslinking and *in situ* HKUST-1 synthesis following a method adapted from Jungho and coworkers. Alginate is a copolymer of mannuronic acid (M unit) and guluronic acid (G unit), arranged in blocks of alternating G and M units. In the presence of Cu²⁺ ions, the G blocks in different alginate chains join together by ionic crosslinking to form a secondary network. Simultaneously, in the presence of the pre-added Lewis base TEA to deprotonate H₃BTC ligands, and the ion-exchangeable sites

on alginate chain, the HKUST-1 MOF is synthesized *in situ* within the hydrogel matrix at room temperature. (Cu²⁺ ions are represented by light blue dots, and HKUST-1 particles are represented by dark blue diamonds in Fig. 1A). Simultaneous cross-linking of the alginate and *in situ* MOF synthesis allows dispersive loading of the MOF and preserves the flexibility of the hydrogel in contrast to alternate methods that dehydrate the hydrogels during synthesis of the MOF.²³

After UV curing, we observed that the printed hydrogel precursor turned into a transparent soft hydrogel with a slight yellowish color as a result of AAm polymerization, and became opaque with a bright blue color after ionic crosslinking and *in situ* HKUST-1 synthesis due to diffusion of Cu²⁺ ions and formation of HKUST-1 crystals. The 3D printed HKUST-1 hydrogel was tough and stretchable, and able to undergo large shape deformation such as elongation up to 453.0% (discussed later).

Rheological properties and printability of hydrogel precursor ink

The rheological properties and printability of the inks are critical for DIW 3D printing. A good DIW ink should exhibit low viscosity and behave like a liquid at high shear rates to allow for extrusion of the ink through the fine printing nozzle. The ink needs to also have high viscosity and show paste-like behavior at low shear rates to preserve the fidelity of 3D shapes after printing. We first investigated the viscosity and viscoelastic properties of a series of hydrogel precursor inks with different shear-thinning agent (HEC) concentrations. We systematically varied the HEC concentration between 2 wt% and 6 wt% and characterized the viscosity and viscoelastic properties of the hydrogel precursor inks. All the hydrogel precursor inks with HEC exhibited a shear-thinning behavior wherein the viscosity of the inks decreased as the shear rate increased (Fig. 2A) and viscoelastic properties (Fig. 2B). Inks with higher HEC concentrations exhibited higher viscosity values across the range of shear rates, and the viscosity increased with increasing HEC

concentration as expected (Fig. 2A). Oscillation tests also indicated shear thinning properties at all concentrations, with larger moduli at higher HEC concentrations. With increasing shear stress, we observed a cross-over between storage and loss modulus, which is an essential feature, the gel point of a DIW ink. Essentially, DIW inks need to show liquid-like behavior that has a higher loss modulus (G") as compared to its storage modulus (G') at high shear stresses. Conversely, at low shear stresses, they need to show solid-like behavior that has a lower loss modulus (G") as compared to its storage modulus (G'),³⁸ which is what we observed for all three HEC concentrations (Fig. 2B).

We also investigated the printability of the inks by printing 30 mm long lines with different HEC concentration and nozzle diameter between 0.4-1.2 mm at different printing pressures between 0 and 260 KPa and generated a printability heat map (Fig. 2C). The blue colored regions indicate the parameter space that results in non-extrudable inks, the white colored regions indicate printable inks, and the pink colored regions indicate inks that do not maintain their shape after printing. We observed that inks with HEC content above 2 wt% were able to retain their shape fidelity after printing with all the nozzle diameters. The inks with 4 wt% HEC exhibited the greatest printability over the working pressures and we used this composition for all our further studies. The relationship between the filament diameter and printing pressure for the 4 wt% HEC ink at different pressures indicates that the diameter increases with increasing pressure (Fig. 2D).

We also characterized the viscosity and viscoelastic properties of inks with different AAm monomer concentrations, as AAm is the major component in our inks other than water (Note S1). The results show that the AAm concentration has a negligible influence on the viscosity and viscoelastic properties of inks, and the printability of inks is not significantly affected by the concentration of AAm in the ink within the range studied.

Characterization and morphology of MOF hydrogel

We characterized the 3D printed hydrogel samples with 4 wt% HEC, with and without the MOF components using X-ray diffraction (XRD), thermogravimetry analysis (TGA), and scanning electron microscopy (SEM). X-ray diffraction confirmed features of the HKUST-1 crystal (Fig. S2). TGA indicated an approximately 6.9 wt % at 800 °C, which we attribute mostly to copper residual constituents. This result suggests adequate Cu²⁺ diffusion into the DN hydrogel matrix (Fig. S3), to ionically cross-link the alginate, and to provide metal ions for HKUST-1 *in situ* growth.

SEM cross-section images of the photocured hydrogel matrix (Fig. 3A) show uniform macropores across the whole cross-section, with a morphology consistent with previously reported AAm gels with HEC.⁴³ After ionic crosslinking and in situ MOF growth, we observed characteristic octahedron shaped HKUST-1 particles distributed relatively uniformly all over the surface (Fig. 3B), external (Fig. 3C) and internal (Fig. 3D) cross-sections of the 3D printed HKUST-1 hydrogel. We attribute high MOF dispersity to the relatively uniform macroporous structure of hydrogel matrix leading to relatively uniformly spaced growth of MOF particles.²¹ Importantly, our *in situ* grown HKUST-1 hydrogel composite shows MOF growth all over the 3D printed samples even in the interior which is an advantage over MOF-polymer composites prepared by directly blending method or surface in situ growth methods. We observed a higher density and smaller crystals (approx. size around 5.5 µm) towards the surface (Fig. 3C) as compared to the bigger particles (approx. size around 10 µm) towards the interior (Fig. 3D). We attribute these differences in density and size distribution of the HKUST-1 particles to differences in the ligand concentration and distribution of Cu²⁺ ions and diffusion limited growth in the bulk, which has also been observed elsewhere.⁴¹

Tunable mechanical properties

An attractive feature of our approach is that we can tune the mechanical properties of the 3D printed MOF hydrogels by varying the relative concentrations of the AAm monomer, covalent and ionic crosslinkers.³⁵ We 3D printed dumbbell-shaped tensile test HKUST-1 hydrogel samples and measured the mechanical properties using a uniaxial tensile test machine following the ASTM D412 standard (Fig. 4A). We observed that the strength, tensile modulus, and toughness of the 3D printed HKUST-1 hydrogels all increased with increasing AAm concentration (Fig. 4C, D). We attribute this increase in mechanical properties to the higher pAAm content in the hydrogel matrix, which leads to elastomer-like properties, which has also been observed in other DN hydrogels.³⁵ In our studies, 3D printed HKUST-1 hydrogels with 3.6 M AAm exhibited the highest failure strain and could be elongated to approximately 453.0% of its original length before breaking. This formulation had a strength of 277.6 kPa, modulus of 152.3 kPa Modulus and toughness of 744.7 kJ/m⁻³.

Alternatively, the mechanical performance of 3D printed HKUST-1 hydrogels can also be adjusted by changing the concentration of the covalent crosslinker MBAA. We observed that the highest strength, strain at break and toughness occurred at a critical concentration of MBAA around 0.06 wt% of AAm (Fig. S4). Our observation is consistent with previous results on DN gels and has been explained by noting that when the MBAA concentration is too low, the polymer network has low crosslinks and the polymer chains are too compliant to hold a shape deformation. Alternatively, when the MBAA concentration is too high, the polymer network is densely crosslinked with short polymer chain segments between crosslinking joints, and thus easier to fracture leading to a decrease of mechanical performance. ³⁵

We also studied the effect of the ionic crosslinker Cu²⁺ concentration contribution to the mechanical properties of the HKUST-1 hydrogel 3D printed samples (Note S4.2). We observed that the tensile modulus increased with increasing Cu²⁺ concentration (Fig. S5B) which can be rationalized by noting that a higher Cu²⁺ concentration leads to a higher extent of ionic crosslinking in the DN hydrogel matrix. We also observed that the strain at break decreased with increasing Cu²⁺ concentration (Fig. S5C) and the maximum strength and toughness occurred at a critical concentration of Cu²⁺ of 0.25 M (Fig. S5B, D). We believe that this optimal concentration is due to the formation of a dense MOF layer towards the surface at high Cu²⁺ concentration beyond the critical point, which would prevent the diffusion of Cu²⁺ ions into and consequently decrease crosslinking in the interior core thereby lowering the strength and toughness. This explanation is consistent with our SEM images which show a variation of MOF particle size distribution and density from the outer surface to the interior core of the 3D printed samples.

Absorption performance of 3D printed MOF hydrogel

Since MOFs are often used for separations, we investigated the performance of our HKUST-1 hydrogel 3D printed shapes to absorb dyes in an aqueous solution. In these tests, we placed a small 3D printed grid scaffold into 10 mL of an aqueous solution containing 30 μM of dye. We examined the absorption of two types of positively charged dyes, methylene blue (MB), rhodamine 6G (R6G), as they have the same charge affinity for non-specific absorption to the DN hydrogel matrix. However, the two dyes have kinetic diameters that are smaller (MB, 7.0 Å) and larger (R6G, 13.0 Å) than the window size (8.5 Å) of HKUST-1 and so it is possible to monitor size-based specific absorption in the MOF component.⁴¹ We continuously monitored the time-dependent absorption of dye by measuring the ultraviolet–visible (UV-Vis) spectra of the solution over 300 minutes (Figure 5). When immersed in single dye solutions, we observed that there was

significant absorption of the smaller sized MB dye in the 3D printed HKUST-1 hydrogel structures illustrating its ability for size-selective absorption (Fig. 5A-F). By collecting the UV-Vis absorbance and converting the values to dye concentrations (Note S5) we can quantify that the 3D printed HKUST-1 hydrogel composite was able to remove 96.3 % of MB, corresponding to a concentration drop from 30.4 μ M to 1.1 μ M. We attribute this high performance in removal rate to the hierarchical porous structure of our printed MOF-hydrogel composites, which combine easy accessibility through macropores, and capillary effects of mesopores, which allow for fast water uptake and large contact surfaces between the MOF micropores and the dyes. In contrast, the R6G concentration dropped from 30.3 μ M to 20.2 μ M with a removal rate of 33.3% and we attribute this removal to non-specific absorption in the DN hydrogel matrix. Importantly, our structures are also able to selectively absorb mainly the MB component from the mixture of the two dyes (Fig. 5G-I).

One of the highlights of 3D DIW printing is the ability to create diverse custom shapes with high diversity, low waste, and versatility. We illustrate this feature by printing three different shapes including a dumbbell (Fig. 6A) for mechanical testing; a pyramid (Fig. 6B), illustrating that the ink retains the shape of a relatively sharp edged structure, and a grid (Fig. 6C), as an example of a high surface area structure or scaffold.

CONCLUSION

In conclusion, we have demonstrated a new 3D DIW printing fabrication method for a highly stretchable *in situ* grown HKUST-1 hydrogel composite of broad relevance to biomedical devices, energy harvesting, robotics, wearables, flexible sensors and separation devices. The pAAm/alginate DN hydrogel acts as a 3D printable porous matrix for facile MOF *in situ* synthesis. The prototypical HKUST-1 3D printed hydrogel structures exhibit high MOF particles dispersity

and excellent mechanical performance. The printed MOF-hydrogel composites can be stretched up to 453.0% of their original length, show high strength of 277.6 kPa, modulus of 152.3 kPa and toughness of 744.7 kJ/m⁻³. Also, the mechanical properties are tunable by adjusting the composition and printing parameters. We believe that the guiding principle used in our methodology could be also used to fabricate flexible composite structures in complex 3D shapes with alternate MOFs families while preserving the performance of MOF. We also anticipate that a similar ink could be utilized with SLA or DLP printers to achieve higher resolution prints.

MATERIALS AND METHODS

Materials

We used at least reagent grade chemicals and solvents as received without further purification. We purchased Acrylamide (AAm), sodium alginate (SA, from brown algae, low viscosity), *N*, *N*'-methylenebis(acrylamide) (MBAA), trimesic acid (H₃BTC), triethylamine (TEA), methylene blue (MB), rhodamine 6G (R6G), acetone, dimethyl sulfoxide (DMSO) from Sigma-Aldrich (USA). According to the vendor, the SA used in this study is typically composed of approximately 61% mannuronic and 39% guluronic acid (M/G ratio ~ 1.56), with a degree of polymerization of 400-600, and molecular weight range between 80,000-120,000. We procured Irgacure 2959 (I2959) from BASF (Switzerland), copper (II) nitrate trihydrate from Fisher Scientific (Poland), and hydroxyethylcellulose (HEC, Natrosol 250HHR) from Ashland (USA). We used deionized water (DI water) for all experiments.

3D printing ink preparation

To prepare the hydrogel precursor inks for 3D printing, we first dissolved SA (1.5 wt% final concentration), H₃BTC (0.05 M final concentration), and TEA (0.15 M final concentration) in water by magnetic stirring at room temperature for a day to form a homogeneous stock solution. Then, we dissolved AAm (0.0 M, 0.9 M, 1.8 M, 3.6 M) and MBAA (0.03 wt%, 0.06 wt%, 0.12 wt% ratio to AAm) in the stock solution to get a series of homogeneous aqueous solutions of various AAm and MBAA concentrations. We added the 50 wt% 12959 DMSO photoinitiator solution into the stock solution to achieve a final 12959 concentration of 0.4 wt% of the ink. We added DI water accordingly to get a series of solutions with the desired concentration. We added the shear-thinning agent HEC (4 wt%, final concentration) in the last step, and stirred the hydrogel precursor solutions at 75 °C for 40 minutes to allow the hydration and gelation of HEC. We kept the hydrogel precursor solutions at room temperature for a day to achieve complete hydration of HEC and to remove air bubbles.

We transferred all the hydrogel precursor inks into UV-blocking cartridges using syringes and centrifuged (IEC CENTRA CL2 centrifuge, Thermo Electron Corporation) them to remove bubbles generated during transfer into cartridges. We stored the prepared precursor inks at room temperature for at least 24 hours to achieve the desired shear thinning properties.

3D printing of hydrogel matrix structure

We loaded the cartridges with the hydrogel precursor inks into a pneumatic extrusion 3D printer (INKREDIB+ 3D Bioprinter, Cellink). We printed the structures using an 18 G (0.8 mm diameter) nozzle on a TeflonTM film covered glass slide at room temperature. The TeflonTM film reduced adhesion of the printed structures on the substrate. We varied the printing pneumatic

pressure between 120 to 150 kPa for the hydrogel inks. We designed all the structures using SolidWorks (Dassault Systèmes) and we exported the designs as STL files. We then sliced the STL files into G-code using the Repetier-Host software via Slic3r slicer. We varied the slicing setting based on each design and we manually edited the G-code as needed.

Post-curing and MOFs in situ synthesis

The curing process for the MOF hydrogel consists of two steps, photocuring, and metal ions cross-linking. We first photocured the 3D printed structures for 15 minutes using an OmniCure UV Curing System (LX 500, Lumen Dynamics) to form a polyacrylamide (pAAm) primary polymer network. To achieve curing, we placed UV LED heads with 365 nm wavelength operating on its 30 % power at a distance of 3 cm from the structure, resulting in a UV intensity of 0.12 W/cm².

We immersed the UV-cured structures into a copper nitrate water acetone (1:1 volume ratio) solution to form a Cu²⁺ cross-linked SA secondary polymer network. Simultaneously, the Cu²⁺ reacted with the MOF forming ligands to *in situ* synthesize the HKUST-1. We kept the UV-cured structures in a series of solutions with varying Cu²⁺ concentrations (0.25 M, 0.50 M, 1.0 M) for 24 hours to allow adequate diffusion of the Cu²⁺ into the hydrogel matrix

Rheology and printability test of the inks

We performed rheology tests on a rotational rheometer (MCR 302, Anton-Paar Instruments) using a parallel plate measuring tool. We kept the temperature of the plate at 25 °C. We measured the viscosity data by rotational tests with shear rates ramping from 0.01 to 1000 s⁻¹. We obtained viscoelasticity data by oscillation tests with shear stress ramping from 0.01 to 1500 Pa.

We conducted printability tests on the 3D printer by printing 30 mm lines on the substrate at different pressures ramping from 0 KPa to 260 KPa, using different sizes of nozzles (16G, 18G, and 22G which correspond to 1.2 mm, 0.8 mm and 0.4 mm inner diameter of the nozzle). We imaged the printed lines and measured their dimensions using ImageJ. We printed three lines for each pressure level and performed all the tests at room temperature.

Mechanical test

We carried out uniaxial tensile tests using a tensile tester (MTS Criterion Series 40, MTS Systems Corporation) equipped with a 100N load cell and used the ASTM D412 standard for our study. We designed dumbbell shaped hydrogel samples with a gauge length of 12 mm, gauge width of 5 mm and 3.2 mm thickness. We printed the samples with rectilinear infill aligned with the loading direction. We measured the dimensions of each tested sample with a caliper before the test. We performed all tests at a constant displacement rate of 10 mm/min and at room temperature. We did at least three duplicate measurements for each sample type and calculated the nominal stress by dividing the tensile force with the initial cross-sectional area of the sample. We defined the strain as the percentage of clamp displacement to the original clamp separation distance. We used the initial linear region of the stress-strain curve between 5 % to 10 % to calculate the elastic modulus. We measured the toughness by integrating the area under the stress-strain curve until the sample fracture point.

Characterization

We obtained powder X-ray diffraction (PXRD) patterns at room temperature using a Bruker D8 Focus diffractometer with a LynxEye detector using Cu K α radiation (λ = 1.5424 A). We freeze-dried the samples and ground them before tests. We used a scanning electron

microscope (SEM, JEOL JSM IT100, JEOL Ltd.) to take images and study the micromorphology of the prepared materials. We freeze dried all the hydrogel samples using a lyophilizer and sputter-coated the samples with a thin layer of gold before imaging. SEM images were obtained at ×1000 magnification (20 kV accelerating voltage). We performed thermogravimetric analysis (TGA) of wet hydrogel samples using a thermogravimetric analyzer (TGA 8000, PerkinElmer Inc.) with a ramp rate of 10 °C/min from 30 °C to 800 °C, under nitrogen flow at the rate of 40 mL/min.

Dye absorption of 3D printed MOFs hydrogel

We carried out the absorption studies of aqueous solutions of MB, R6G dyes in a batch experiment at room temperature. We prepared HKUST-1 hydrogel grid scaffolds with design dimensions of 20 mm x 20 mm x 4 mm and measured the weight of the scaffolds using an analytical balance before the absorption tests. Typically, we added one scaffold to 10 mL of aqueous dye solution with an initial concentration of 30 µM. After absorption for a period of time, we shook the sample bottles, and poured the solution into a quartz cuvette for analysis. We returned the solution in the cuvette to the sample bottle to continue the test. We monitored the dye absorption process using a UV-Vis spectrophotometer (Lambda 950, PerkinElmer Inc.) over 300 minutes. We recorded the UV-vis spectra of dye solutions between wavelengths of 400 to 800 nm with a scanning interval of 5 nm, and quantified the MB, R6G concentrations by measuring the absorbance peaks at 660 nm and 525 nm respectively.

ASSOCIATED CONTENT

Supporting Information

The Supporting Information (SI) is available free of charge on the ACS Publications website at DOI:

The SI includes: Supplementary rheological and printability test of inks, XRD pattern of 3D printed hydrogel samples, TGA profiles of 3D printed hydrogel samples, supplementary mechanical test, and dye absorption test results.

AUTHOR INFORMATION

Corresponding Author

*E-mail: dgracias@jhu.edu.

Author Contributions

W. L. conceived the research design and conducted the experiments; D.H.G., and O. E. supervised the experiments and the study; O.E. provided suggestions on designs and mechanical tests; W.L. and D.H.G. wrote the manuscript with input and edits from O.E.

ACKNOWLEDGMENTS

We acknowledge support from the National Science Foundation Grant EFMA-1830893

References

- (1) Li, H.; Eddaoudi, M.; O'Keeffe, M.; Yaghi, O. M. Design and Synthesis of an Exceptionally Stable and Highly Porous Metal-Organic Framework. *Nature*. **1999**, 402, 276–279.
- (2) Kirchon, A.; Feng, L.; Drake, H. F.; Joseph, E. A.; Zhou, H.-C. From Fundamentals to Applications: A Toolbox for Robust and Multifunctional MOF Materials. *Chem. Soc. Rev.* **2018**, *47*, 8611–8638.
- (3) Silva, P.; Vilela, S. M. F.; Tomé, J. P. C.; Almeida Paz, F. A. Multifunctional Metal–Organic Frameworks: From Academia to Industrial Applications. *Chem. Soc. Rev.* **2015**, *44*, 6774–6803.
- (4) Wang, L.; Fang, M.; Liu, J.; He, J.; Li, J.; Lei, J. Layer-by-Layer Fabrication of High-Performance Polyamide/ZIF-8 Nanocomposite Membrane for Nanofiltration Applications. *ACS Appl. Mater. Interfaces* **2015**, *7*, 24082–24093.
- (5) Dai, J.; Li, S.; Liu, J.; He, J.; Li, J.; Wang, L.; Lei, J. Fabrication and Characterization of a Defect-Free Mixed Matrix Membrane by Facile Mixing PPSU with ZIF-8 Core–shell Microspheres for Solvent-Resistant Nanofiltration. *J. Membr. Sci.* **2019**, *589*, 117261.
- (6) Millward, A. R.; Yaghi, O. M. Metal–Organic Frameworks with Exceptionally High Capacity for Storage of Carbon Dioxide at Room Temperature. *J. Am. Chem. Soc.* **2005**, *127*, 17998–17999.
- (7) Wang, D.; Zhou, J.; Chen, R.; Shi, R.; Xia, G.; Zhou, S.; Liu, Z.; Zhang, N. Q.; Wang, H.; Guo, Z.; Chen, Q. Magnetically Guided Delivery of DHA and Fe Ions for Enhanced Cancer Therapy Based on PH-Responsive Degradation of DHA-Loaded Fe₃O₄@C@MIL-100(Fe) Nanoparticles. *Biomaterials* **2016**, *107*, 88–101.
- (8) He, M.; Zhou, J.; Chen, J.; Zheng, F.; Wang, D.; Shi, R.; Guo, Z.; Wang, H.; Chen, Q. Fe₃O₄ @carbon@zeolitic Imidazolate Framework-8 Nanoparticles as Multifunctional pH-Responsive Drug Delivery Vehicles for Tumor Therapy *in vivo. J. Mater. Chem. B Mater. Biol. Med.* **2015**, *3*, 9033–9042.
- (9) Liu, J.; He, J.; Wang, L.; Li, R.; Chen, P.; Rao, X.; Deng, L.; Rong, L.; Lei, J. NiO-PTA Supported on ZIF-8 as a Highly Effective Catalyst for Hydrocracking of Jatropha Oil. *Sci. Rep.* **2016**, *6*, 23667.
- (10) Liu, J.; Sun, F.; Zhang, F.; Wang, Z.; Zhang, R.; Wang, C.; Qiu, S. In Situ Growth of Continuous Thin Metal—organic Framework Film for Capacitive Humidity Sensing. *J. Mater. Chem.* **2011**, *21*, 3775-3778.
- (11) Tu, M.; Wannapaiboon, S.; Khaletskaya, K.; Fischer, R. A. Engineering Zeolitic-Imidazolate Framework (ZIF) Thin Film Devices for Selective Detection of Volatile Organic Compounds. *Adv. Funct. Mater.* **2015**, *25*, 4470–4479.
- (12) Senkovska, I.; Kaskel, S. Ultrahigh Porosity in Mesoporous MOFs: Promises and Limitations. *ChemComm.* **2014**, *50* 7089-7098.
- (13) Huang, N.; Drake, H.; Li, J.; Pang, J.; Wang, Y.; Yuan, S.; Wang, Q.; Cai, P.; Qin, J.; Zhou, H.-C. Flexible and Hierarchical Metal-Organic Framework Composites for High-Performance Catalysis. *Angew. Chem. Int. Ed Engl.* **2018**, *57*, 8916–8920.
- (14) Li, S.; Huo, F. Metal–organic Framework Composites: From Fundamentals to Applications. *Nanoscale*. **2015**, *7*, 7482–7501.
- (15) Rui, K.; Wang, X.; Du, M.; Zhang, Y.; Wang, Q.; Ma, Z.; Zhang, Q.; Li, D.; Huang, X.; Sun, G.; Zhu, J.; Huang, W. Dual-Function Metal-Organic Framework-Based Wearable Fibers for Gas Probing and Energy Storage. *ACS Appl. Mater. Interfaces* **2018**, *10*, 2837–2842.
- (16) Ling, W.; Liew, G.; Li, Y.; Hao, Y.; Pan, H.; Wang, H.; Ning, B.; Xu, H.; Huang, X. Materials and Techniques for Implantable Nutrient Sensing Using Flexible Sensors Integrated with Metal-Organic Frameworks. *Adv. Mater.* **2018**, *30*, e1800917.
- (17) Troyano, J.; Carné-Sánchez, A.; Pérez-Carvajal, J.; León-Reina, L.; Imaz, I.; Cabeza, A.; Maspoch, D. A Self-Folding Polymer Film Based on Swelling Metal-Organic Frameworks. *Angew. Chem. Int. Ed Engl.* **2018**, *57*, 15420–15424.
- (18) Xu, X.; Shi, W.; Li, P.; Ye, S.; Ye, C.; Ye, H.; Lu, T.; Zheng, A.; Zhu, J.; Xu, L.; Zhong, M.; Cao,

- X. Facile Fabrication of Three-Dimensional Graphene and Metal—Organic Framework Composites and Their Derivatives for Flexible All-Solid-State Supercapacitors. *Chem. Mater.* **2017**, *29*, 6058–6065.
- (19) Gong, J.; Xu, Z.; Tang, Z.; Zhong, J.; Zhang, L. Highly Compressible 3-D Hierarchical Porous Carbon Nanotube/metal Organic Framework/polyaniline Hybrid Sponges Supercapacitors. *AIP Adv.* **2019**, *9*, 055032.
- (20) Zhang, K.; Huo, Q.; Zhou, Y.-Y.; Wang, H.-H.; Li, G.-P.; Wang, Y.-W.; Wang, Y.-Y. Textiles/Metal-Organic Frameworks Composites as Flexible Air Filters for Efficient Particulate Matter Removal. *ACS Appl. Mater. Interfaces.* **2019**, *11*, 17368–17374.
- (21) Zhu, H.; Yang, X.; Cranston, E. D.; Zhu, S. Flexible and Porous Nanocellulose Aerogels with High Loadings of Metal-Organic-Framework Particles for Separations Applications. *Adv. Mater.* **2016**, *28*, 7652–7657.
- (22) Richardson, J. J.; Tardy, B. L.; Guo, J.; Liang, K.; Rojas, O. J.; Ejima, H. Continuous Metal–Organic Framework Biomineralization on Cellulose Nanocrystals: Extrusion of Functional Composite Filaments. *ACS Sustain. Chem. Eng.* **2019**, *7*, 6287–6294.
- (23) Zhu, H.; Zhang, Q.; Zhu, S. Alginate Hydrogel: A Shapeable and Versatile Platform for in Situ Preparation of Metal-Organic Framework-Polymer Composites. *ACS Appl. Mater. Interfaces.* **2016**, 8, 17395–17401.
- (24) Dai, J.; Xiao, S.; Liu, J.; He, J.; Lei, J.; Wang, L. Fabrication of ZIF-9@super-Macroporous Microsphere for Adsorptive Removal of Congo Red from Water. *RSC Adv.* **2017**, *7*, 6288–6296.
- (25) Lipson, H.; Kurman, M. *Fabricated: The New World of 3D Printing*; John Wiley & Sons: Hoboken **2013**.
- (26) Shi, Z.; Xu, C.; Chen, F.; Wang, Y.; Li, L.; Meng, Q.; Zhang, R. Renewable Metal-organic-Frameworks-Coated 3D Printing Film for Removal of Malachite Green. *RSC Adv.* **2017**, *7*, 49947–49952.
- (27) Wang, Z.; Wang, J.; Li, M.; Sun, K.; Liu, C.-J. Three-Dimensional Printed Acrylonitrile Butadiene Styrene Framework Coated with Cu-BTC Metal-Organic Frameworks for the Removal of Methylene Blue. *Sci. Rep.* **2014**, *4*, 5939.
- (28) Halevi, O.; Tan, J. M. R.; Lee, P. S.; Magdassi, S. Hydrolytically Stable MOF in 3D-Printed Structures. *Adv. Sustain. Syst.* **2018**, *2*, 1700150.
- (29) Thakkar, H.; Eastman, S.; Al-Naddaf, Q.; Rownaghi, A. A.; Rezaei, F. 3D-Printed Metal-Organic Framework Monoliths for Gas Adsorption Processes. *ACS Appl. Mater. Interfaces.* **2017**, *9*, 35908–35916.
- (30) Bible, M.; Sefa, M.; Fedchak, J. A.; Scherschligt, J.; Natarajan, B.; Ahmed, Z.; Hartings, M. R. 3D-Printed Acrylonitrile Butadiene Styrene-Metal Organic Framework Composite Materials and Their Gas Storage Properties. *3D Print Addit. Manuf.* **2018**, *5*, 63–72.
- (31) Sultan, S.; Abdelhamid, H. N.; Zou, X.; Mathew, A. P. CelloMOF: Nanocellulose Enabled 3D Printing of Metal-Organic Frameworks. *Adv. Funct. Mater.* **2019**, *29*, 1805372.
- (32) Lyu, Z.; Lim, G. J. H.; Guo, R.; Kou, Z.; Wang, T.; Guan, C.; Ding, J.; Chen, W.; Wang, J. 3D-Printed MOF-Derived Hierarchically Porous Frameworks for Practical High-Energy Density Li-O2 Batteries. *Adv. Funct. Mater.* **2019**, *29*, 1806658.
- (33) Knebel, A.; Friebe, S.; Bigall, N. C.; Benzaqui, M.; Serre, C.; Caro, J. Comparative Study of MIL-96(Al) as Continuous Metal-Organic Frameworks Layer and Mixed-Matrix Membrane. *ACS Appl. Mater. Interfaces.* **2016**, *8*, 7536–7544.
- (34) Zhang, M.; Li, L.; Lin, Q.; Tang, M.; Wu, Y.; Ke, C. Hierarchical-Coassembly-Enabled 3D-Printing of Homogeneous and Heterogeneous Covalent Organic Frameworks. *J. Am. Chem. Soc.* **2019**, *141*, 5154–5158.
- (35) Sun, J.-Y.; Zhao, X.; Illeperuma, W. R. K.; Chaudhuri, O.; Oh, K. H.; Mooney, D. J.; Vlassak, J. J.; Suo, Z. Highly Stretchable and Tough Hydrogels. *Nature*. **2012**, *489*, 133–136.
- (36) Liu, J.; Erol, O.; Pantula, A.; Liu, W.; Jiang, Z.; Kobayashi, K.; Chatterjee, D.; Hibino, N.; Romer, L. H.; Kang, S. H.; Nguyen, T. D.; Gracias, D. H. Dual-Gel 4D Printing of Bioinspired Tubes. *ACS*

- Appl. Mater. Interfaces 2019, 11, 8492-8498.
- (37) Liu, J.; Liu, W.; Pantula, A.; Wang, Z.; Gracias, D. H.; Nguyen, T. D. Periodic Buckling of Soft 3D Printed Bioinspired Tubes. *Extreme Mech. Lett.* **2019**, *30*, 100514.
- (38) Jiang, Z.; Erol, O.; Chatterjee, D.; Xu, W.; Hibino, N.; Romer, L. H.; Kang, S. H.; Gracias, D. H. Direct Ink Writing of Poly(tetrafluoroethylene) (PTFE) with Tunable Mechanical Properties. *ACS Appl. Mater. Interfaces.* **2019**, *11*, 28289-28295.
- (39) Boutelier, D.; Cruden, A.; Saumur, B. Density and Visco-Elasticity of Natrosol 250 HH Solutions: Determining Their Suitability for Experimental Tectonics. *J. Struct. Geol.* **2016**, *86*, 153–165.
- (40) Yang, C. H.; Wang, M. X.; Haider, H.; Yang, J. H.; Sun, J.-Y.; Chen, Y. M.; Zhou, J.; Suo, Z. Strengthening Alginate/polyacrylamide Hydrogels Using Various Multivalent Cations. *ACS Appl. Mater. Interfaces* **2013**, *5*, 10418–10422.
- (41) Lim, J.; Lee, E. J.; Choi, J. S.; Jeong, N. C. Diffusion Control in the *in situ* Synthesis of Iconic Metal-Organic Frameworks within an Ionic Polymer Matrix. *ACS Appl. Mater. Interfaces* **2018**, *10*, 3793–3800.
- (42) Zhang, Z.; Jin, Y.; Yin, J.; Xu, C.; Xiong, R.; Christensen, K.; Ringeisen, B. R.; Chrisey, D. B.; Huang, Y. Evaluation of Bioink Printability for Bioprinting Applications. *Appl. Phys. Rev.* **2018**, *5*, 041304.
- (43) Zhang, T.; Zuo, T.; Hu, D.; Chang, C. Dual Physically Cross-Linked Nanocomposite Hydrogels Reinforced by Tunicate Cellulose Nanocrystals with High Toughness and Good Self-Recoverability. *ACS Appl. Mater. Interfaces* **2017**, *9*, 24230–24237.

Figures and figure captions

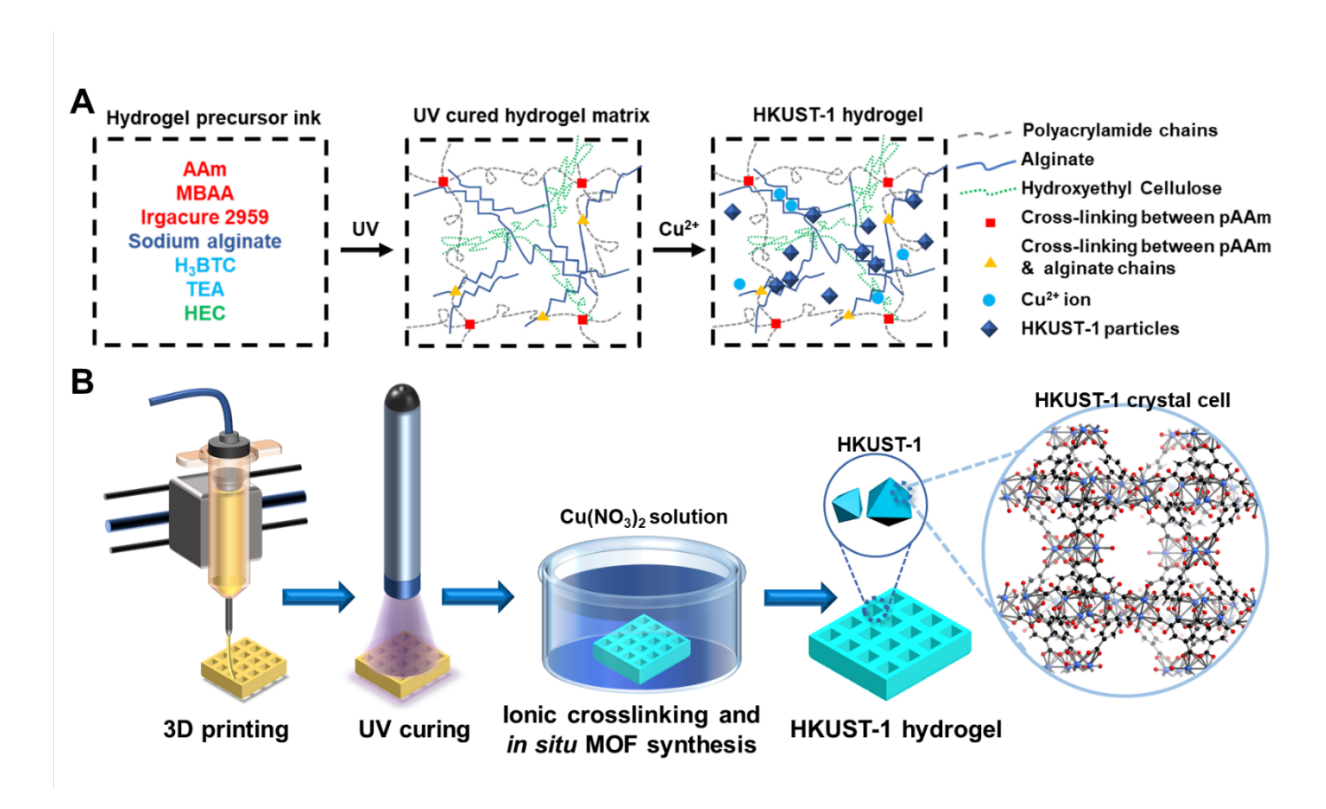


Figure 1. Schematics of the chemical composition and 3D printing process for the MOF hydrogel structures. (A) Composition of the hydrogel precursor ink (left), UV cured hydrogel matrix (middle), and the HKUST-1 hydrogel (right). (B) Schematic showing the three critical steps in the 3D printing process including printing, UV curing and ionic crosslinking.

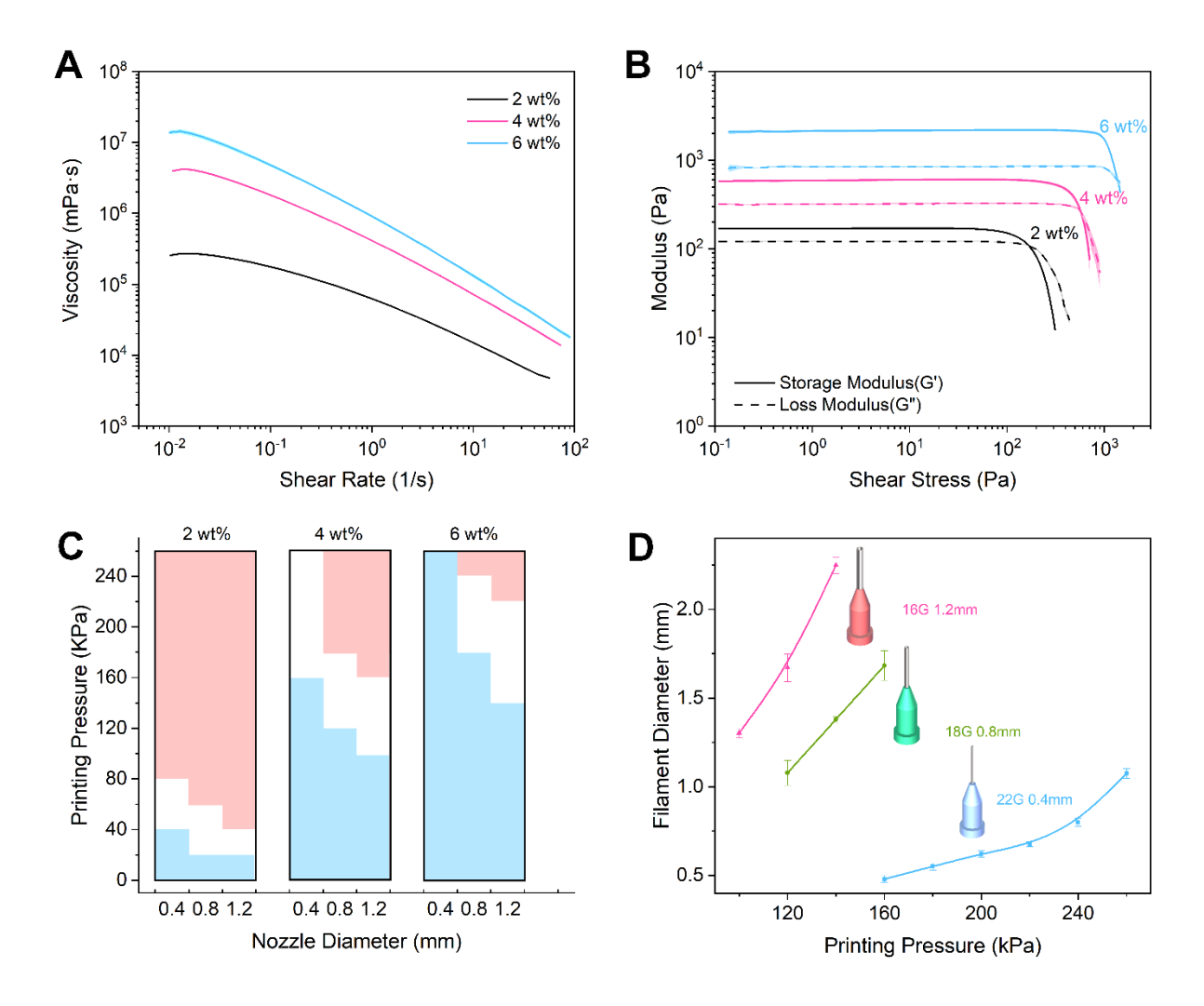


Figure 2. Printability and rheological characteristics of the hydrogel precursor inks (A) Plot of the viscosity of the inks as a function of shear rate with different HEC concentrations. **(B)** Plot of the storage and loss moduli of the inks as a function of shear stress with different HEC concentrations. **(C)** Printability heat map of the inks with varying HEC concentrations, printer nozzle and printing pressure. The blue regions indicate non-extrudable inks, white regions represent printable inks and pink regions represent overextruding regions where the printing extrusion velocity is too high to retain the shape fidelity of prints. **(D)** Plot of the printed filament diameters for the 4 wt% HEC ink as a function of printing pressure for different nozzle diameters.

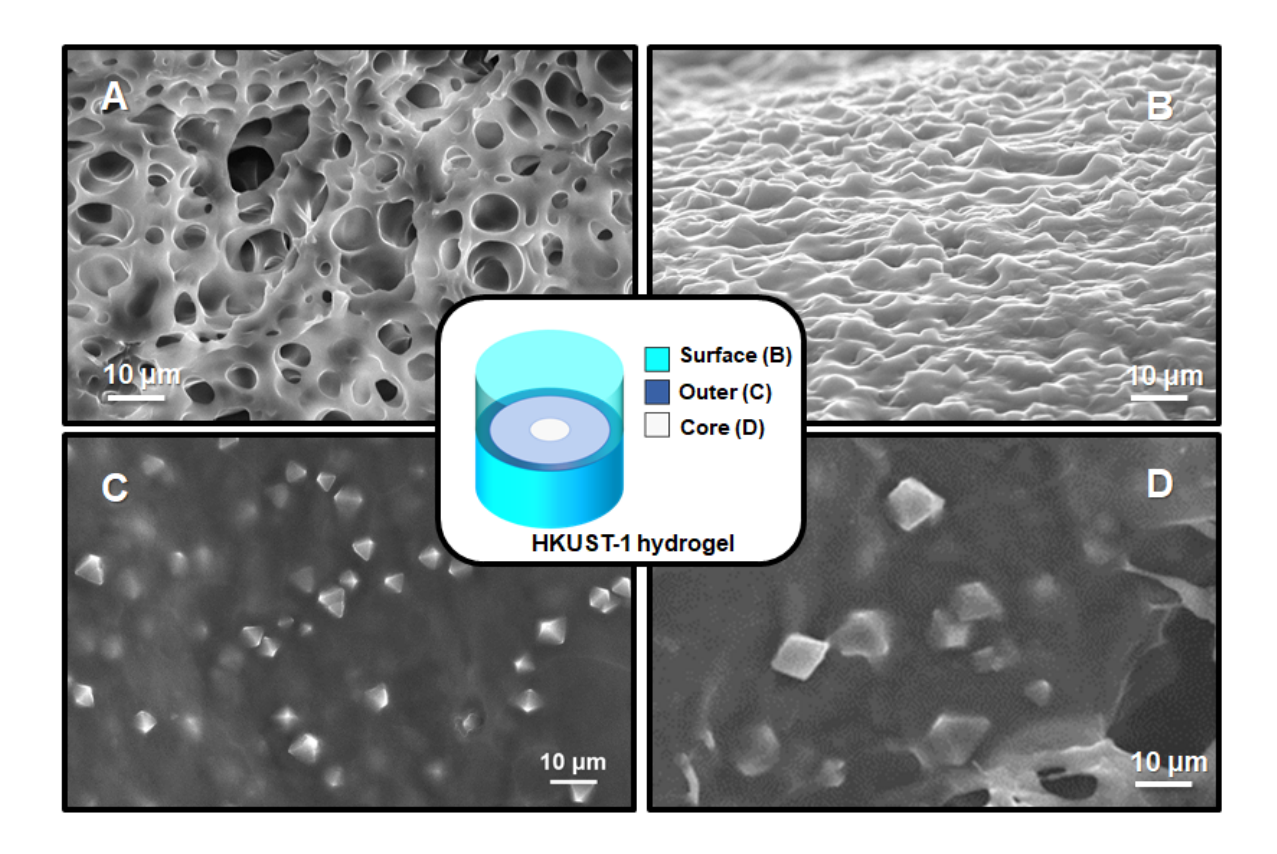


Figure 3. SEM images of the 3D printed hydrogel samples. (A) Cross-section SEM image of the 3D printed and photocured hydrogel matrix. **(B)** SEM image of the surface of the 3D printed HKUST-1 hydrogel. **(C-D)** Cross-section SEM images of the 3D printed HKUST-1 hydrogel, **(C)** towards the outer region and **(D)** at core region.

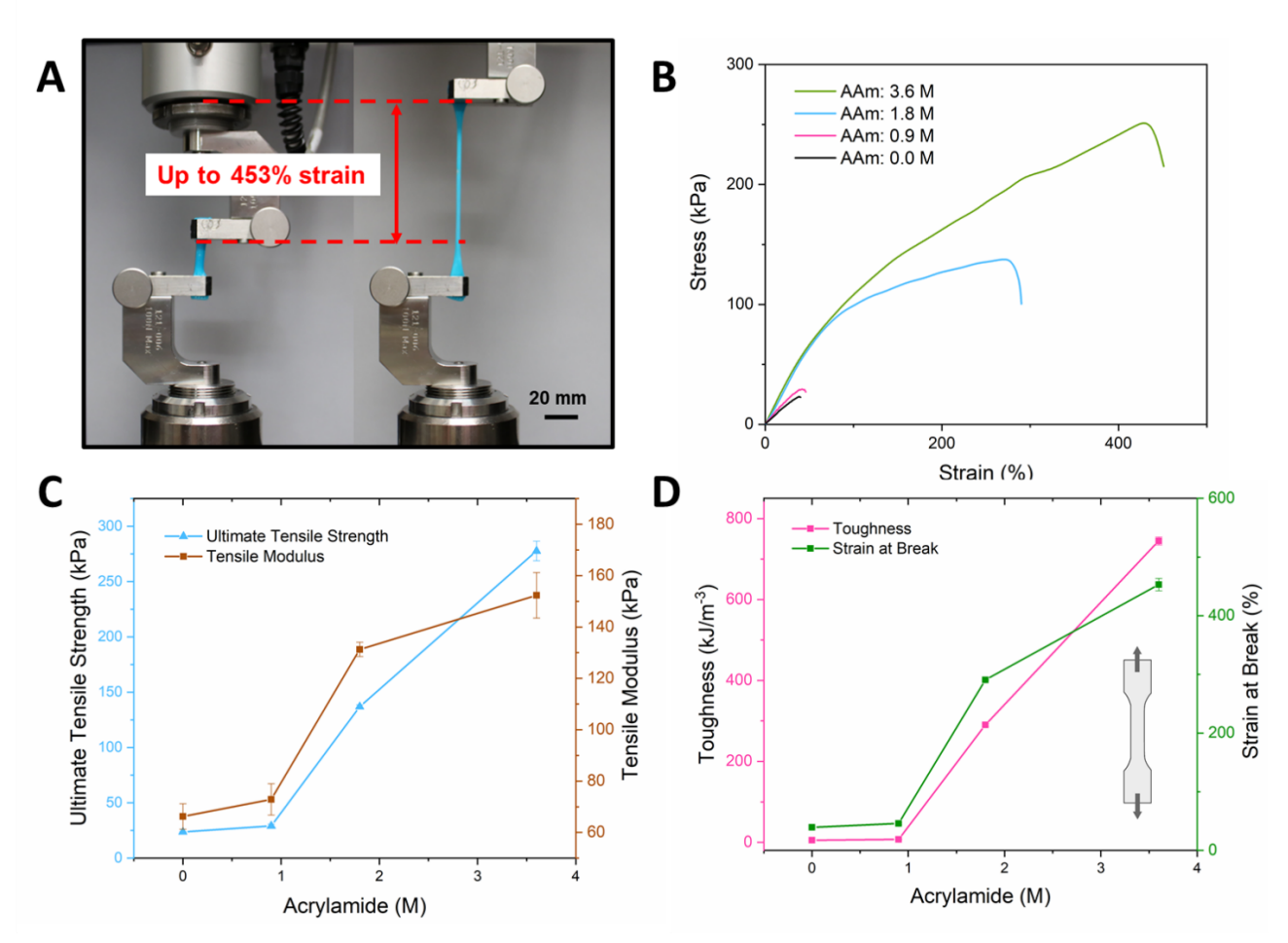


Figure 4. Mechanical properties of the 3D printed HKUST-1 hydrogels with different AAm concentrations (A) Optical images showing the mechanical testing of the 3D printed HKUST-1 dumbbell shape sample. (B) Plot of the stress-strain curves. (C) Plot of the ultimate tensile strength and tensile modulus as a function of the AAm concentration. (D) Plot of the strain at break and toughness as a function of the AAm concentration.

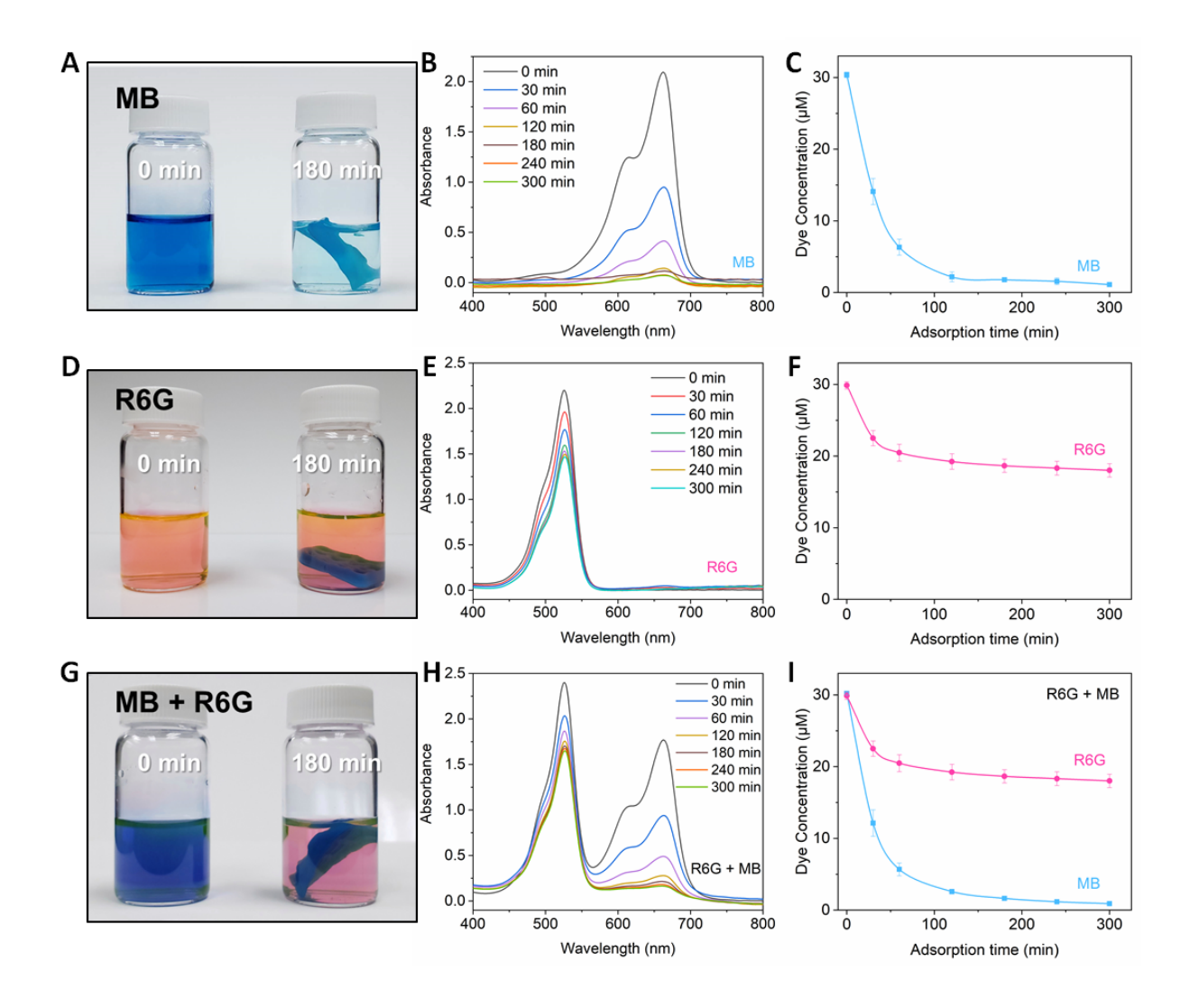


Figure 5. Dye absorption performance of the 3D printed HKUST-1 hydrogels. Optical images of vials of dye solutions before and after absorption for **(A)** MB, **(D)** R6G, and **(G)** MB + R6G. Time-dependent UV-vis absorbance spectra for aliquots from **(B)** HKUST-1 hydrogel immersed in MB, **(E)** HKUST-1 hydrogel immersed in R6G, and **(H)** HKUST-1 hydrogel immersed in MB + R6G. Plot of the time-dependent dye concentration obtained from the UV-vis spectra for aliquots from **(C)** HKUST-1 hydrogel immersed in MB, **(F)** HKUST-1 hydrogel immersed in R6G, and **(I)** HKUST-1 hydrogel immersed in MB + R6G solutions.

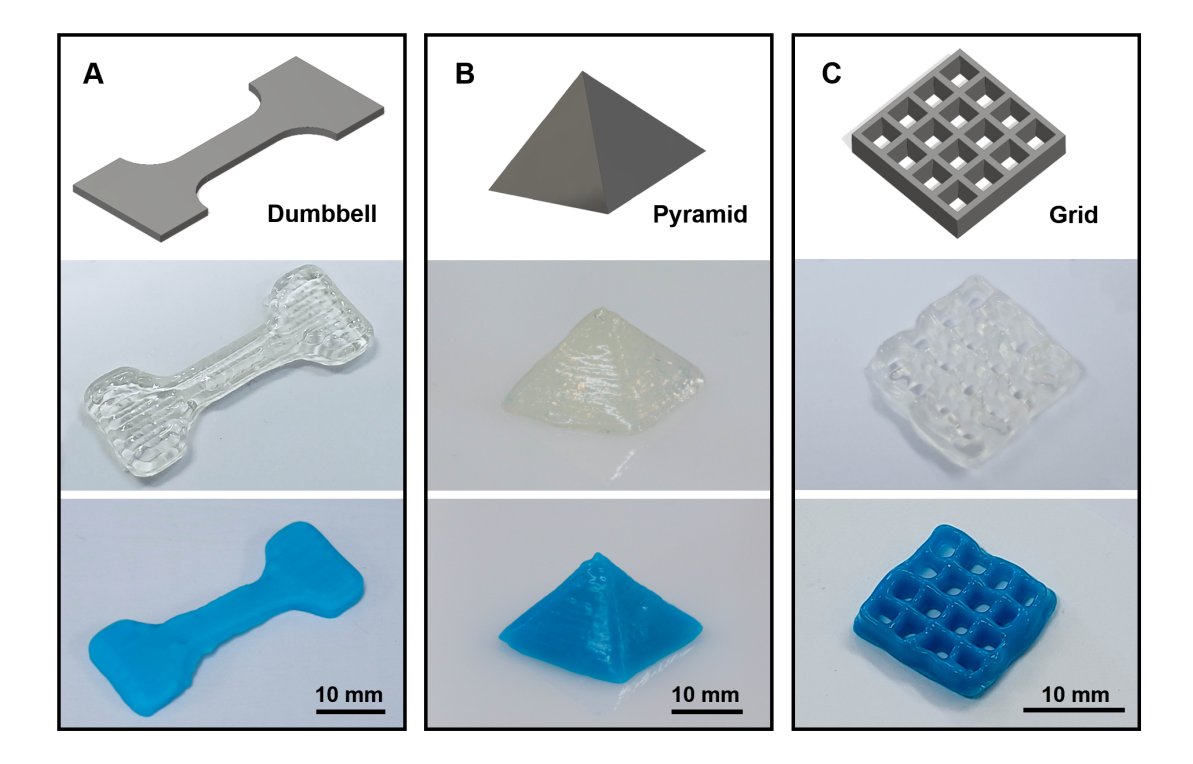
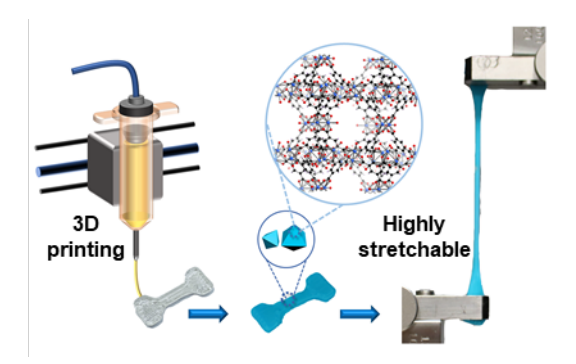


Figure 6. Examples of 3D printed MOF-hydrogel composites in different shapes. (A-C) 3D renderings (top), and optical images of 3D printed hydrogel matrix samples (middle) and 3D printed HKUST-1 hydrogel samples (bottom) with a variety of shapes printed with a 0.8 mm diameter nozzle. **(A)** Dumbbell, **(B)** pyramid, and **(C)** grid.

TOC Figure



Supporting Information

3D Printing of an *In situ* Grown MOF Hydrogel with Tunable Mechanical Properties

Wangqu Liu¹, Ozan Erol², David H. Gracias^{1,3,4*}

*Corresponding author: dgracias@jhu.edu

Table of Contents

Note S1. Rheological and printability test of the hydrogel precursor inks	S2
Note S2. X-ray diffraction scan of the 3D printed hydrogel samples	S3
Note S3. Thermogravimetry analysis of the 3D printed hydrogel samples	S4
Note S4. Mechanical test results	S5
S4.1 Mechanical testing of 3D printed HKUST-1 hydrogels with different MBAA concentrations S4.2 Mechanical test of 3D printed HKUST-1 hydrogels processed by solutions with different Cu ²⁺ concentration	S5 + S6
Note S5. Dye absorption tests	S7
S5.1 Baseline setup for dye solutions	S7
S5.2 Dye absorption performance of 3D printed HKUST-1 hydrogel with different AAm concentrations	S8
References	S9

¹ Department of Chemical & Biomolecular Engineering Johns Hopkins University, 3400 North Charles Street, Baltimore, Maryland 21218, United States

² Department of Mechanical Engineering and Hopkins Extreme Materials Institute Johns Hopkins University, 3400 North Charles Street, Baltimore, Maryland 21218, United States

³ Department of Materials Science and Engineering Johns Hopkins University, 3400 North Charles Street, Baltimore, Maryland 21218, United States

⁴ Department of Chemistry Johns Hopkins University, 3400 North Charles Street, Baltimore, Maryland 21218, United States

Note S1. Rheological and printability test of the hydrogel precursor inks

We tested the rheological properties of the hydrogel precursor inks by varying the concentration of acrylamide (AAm) and keeping the concentration of the shear-thinning agent hydroxyethylcellulose (HEC) concentration at 4 wt%. All the inks with HEC exhibited a shear-thinning behavior as expected, and all the plots of viscosity vs shear rate were similar (Fig. S1A). As for the storage/loss modulus vs shear stress (Fig. S1B), we observed the presence of a gel point among all inks. Inks with AAm exhibited higher storage/loss moduli than the ink without AAm, but there was little variation between 0.9, 1.8 and 3.6 M samples. The printability tests in Fig. 2C and 2D were conducted by printing 30 mm long lines on the substrate (Fig. S1C).

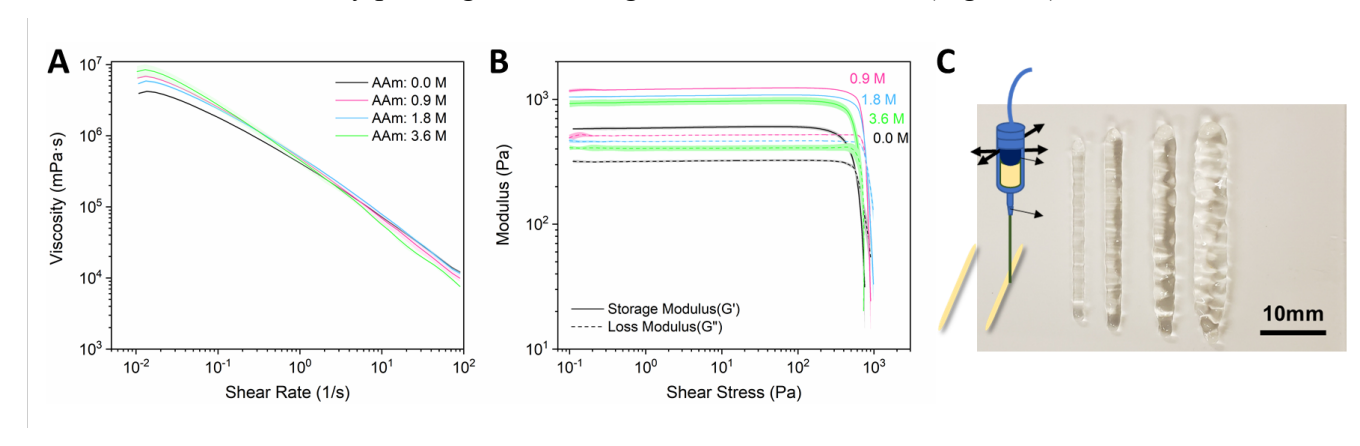


Figure S1. (A) Plot of the viscosity of the inks as a function of shear rate for different AAm concentrations. **(B)** Plot of the storage and loss moduli of the inks as a function of shear stress for different AAm concentrations. **(C)** Optical image of approximately 30 mm long 3D printed lines with increasing printing pressure from the left to right.

Note S2. X-ray diffraction scan of the 3D printed hydrogel samples

The XRD diffractogram of 3D printed hydrogel samples is shown in Fig. S2. The gray line is the simulated HKUST-1 XRD diffractogram obtained from published data on The Cambridge Crystallographic Data Centre (CCDC).¹ The orange line is our measured XRD diffractogram for the freeze dried 3D printed hydrogel matrix before ionic cross-linking and *in situ* MOF synthesis. and the blue line is our measured XRD diffractogram for the freeze-dried 3D printed HKUST-1 hydrogel (1.8 M AAm, 4 wt% HEC, 0.5 M Cu²⁺). We observed features of the HKUST-1 MOF within the freeze-dried 3D printed HKUST-1 hydrogel. The signal to noise ratio is a consequence of environmental moisture and the scan rate. ^{2,3}

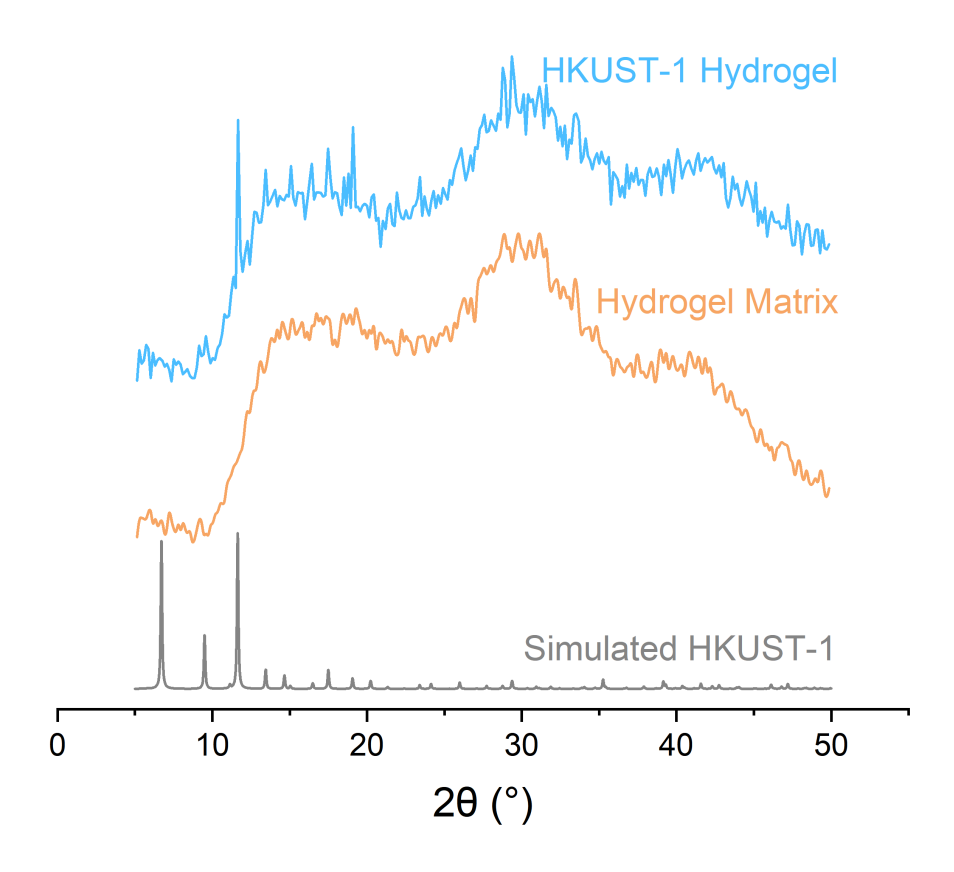


Figure S2. XRD pattern of the samples.

Note S3. Thermogravimetry analysis of the 3D printed hydrogel samples

To analyze the loading efficiency of the 3D printed HKUST-1 hydrogel, we performed thermogravimetry analysis (TGA) for the HKUST-1 hydrogel (1.8 M AAm, 4 wt% HEC, 0.5 M Cu²⁺) and the hydrogel matrix (1.8 M AAm, 4 wt% HEC). The TGA results are shown in Fig. S3A; the pink line and the gray line represent the HKUST-1 hydrogel and the hydrogel matrix, respectively, and the shadow indicates standard error. We observed that the hydrogel matrix almost completely degrades after heating to 800 °C, while the HKUST-1 hydrogel composite has a residual weight of about 6.9 wt%. We attribute the residue mainly to CuO and small amounts of carbon.⁴ The TGA result indicates that sufficient Cu²⁺ diffused into the hydrogel matrix. We also observed that the degradation peaks of the HKUST-1 hydrogel shift to the right side compared to the hydrogel matrix in derivative thermogravimetry (DTG, Fig. S3B), indicating that the secondary ionic crosslinking and MOF growth improve the thermal stability of the hydrogel composite.⁵

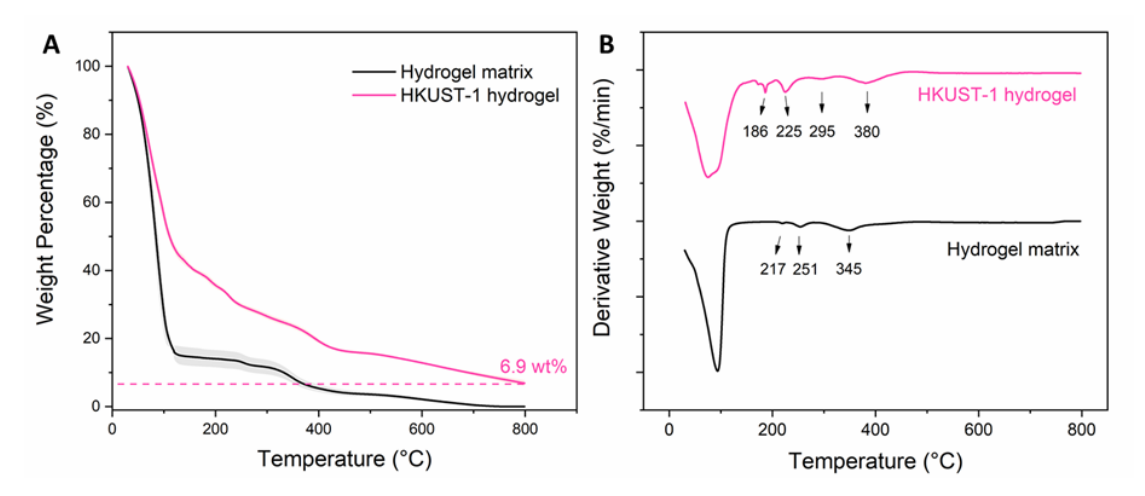


Figure S3. TGA scans of the samples. The pink lines represent the 3D printed HKUST-1 hydrogel, the grey lines represent the hydrogel matrix. (A) Thermogravimetric analysis (TGA), and (B) derivative thermo-gravimetric (DTG) plot of the 3D printed HKUST-1 hydrogel and the hydrogel matrix.

Note S4. Mechanical test results

S4.1 Mechanical testing of 3D printed HKUST-1 hydrogels with different MBAA concentrations

To study the effects of covalent cross-linker concentration, we prepared and measured the mechanical properties of 3D printed HKUST-1 hydrogels with different concentrations of N,N'-methylenebis(acrylamide) (MBAA) ranging from 0.03 wt% to 0.12 wt% of AAm. All these samples had the same AAm concentration at 1.8 M, HEC concentration at 4 wt% and Cu^{2+} concentration at 0.5 M.

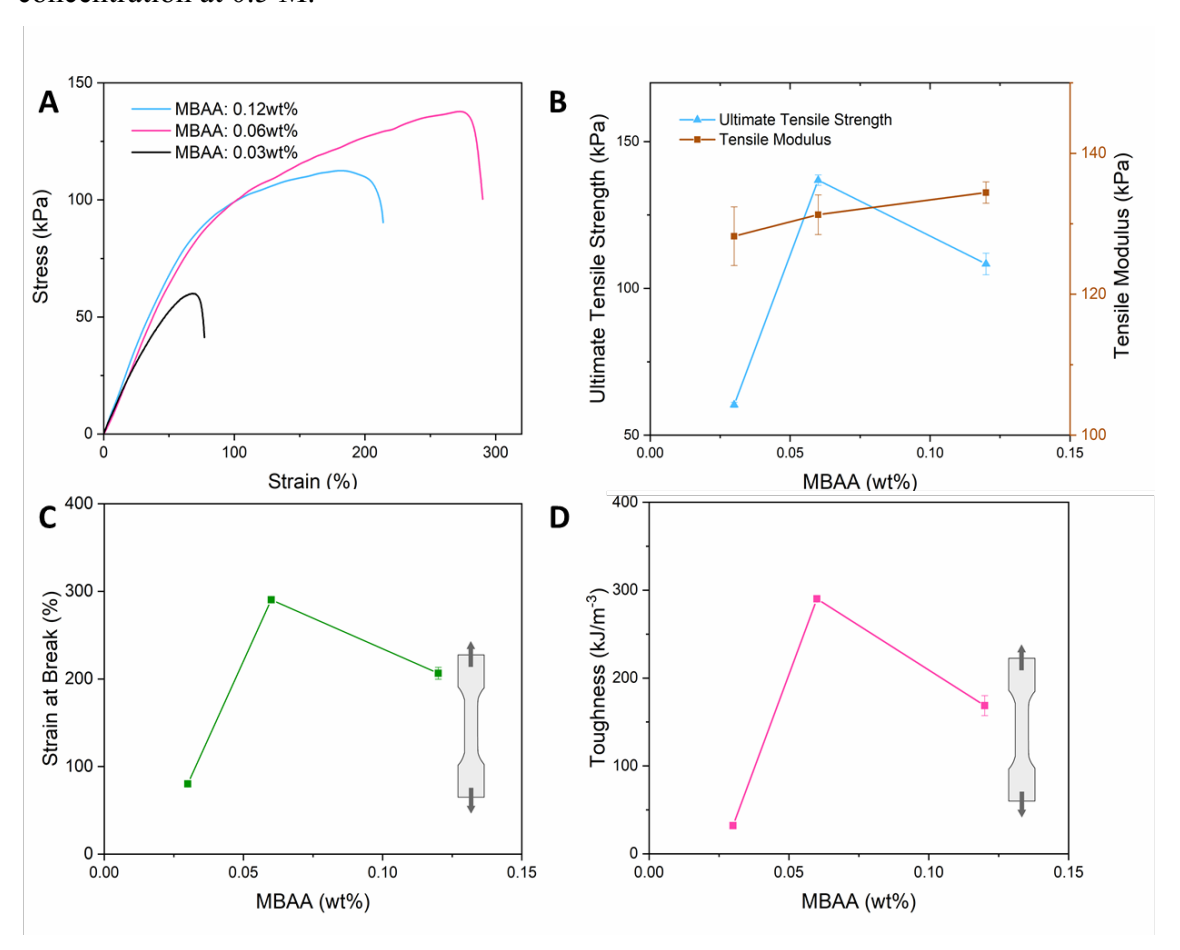


Figure S4. Mechanical properties of 3D printed HKUST-1 hydrogels with different MBAA concentrations. (A) Plot of stress-strain curves. (B) Plot of ultimate tensile strength and tensile modulus as a function of MBAA concentration. (C) Plot of strain at break as a function of MBAA concentration. (D) Plot of toughness as a function of MBAA concentration.

S4.2 Mechanical test of 3D printed HKUST-1 hydrogels processed by solutions with different Cu^{2+} concentration

To examine the influence of the ionic cross-linker concentration, we prepared and measured the mechanical properties of 3D printed HKUST-1 hydrogels crosslinked with different Cu²⁺ concentrations ranging from 0 M to 1 M. All these samples had the same AAm concentration at 1.8M, the HEC concentration at 4 wt% and the MBAA concentration at 0.06 wt% of AAm.

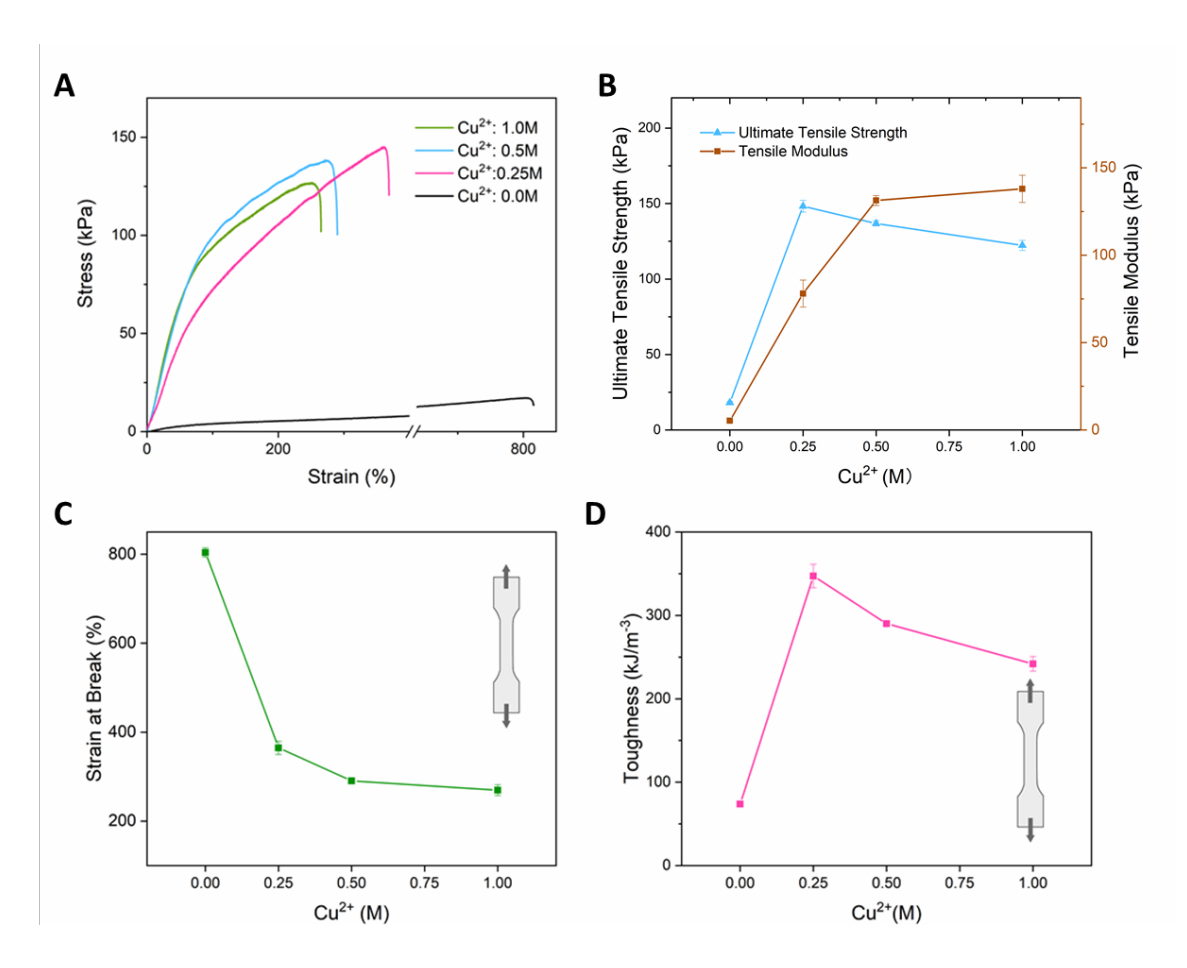


Figure S5. Mechanical properties of 3D printed HKUST-1 hydrogels processed by solutions with different Cu^{2+} concentration (A) Plot of stress-strain curves. (B) Plot of ultimate tensile strength and tensile modulus as a function of Cu^{2+} concentration. (C) Plot of strain at break as a function of Cu^{2+} concentration. (D) Plot of toughness as a function of Cu^{2+} concentration.

Note S5. Dye absorption tests

S5.1 Baseline setup for dye solutions

To quantitatively analyze the dye absorption of 3D printed HKUST-1 hydrogel samples, we prepared a series of solutions of methylene blue (MB), rhodamine 6G (R6G) with concentrations ranging from 1 μ M to 30 μ M to set up the baselines. We recorded the UV-Vis spectra of these solutions (Fig. S6A, C), and plotted the dye concentrations as a function of absorbance at the highest points to get the baselines (Fig. S6B, D), the MB and R6G have the extinction coefficients of 14.38 μ M⁻¹nm⁻¹ and 14.08 μ M⁻¹nm⁻¹, respectively.

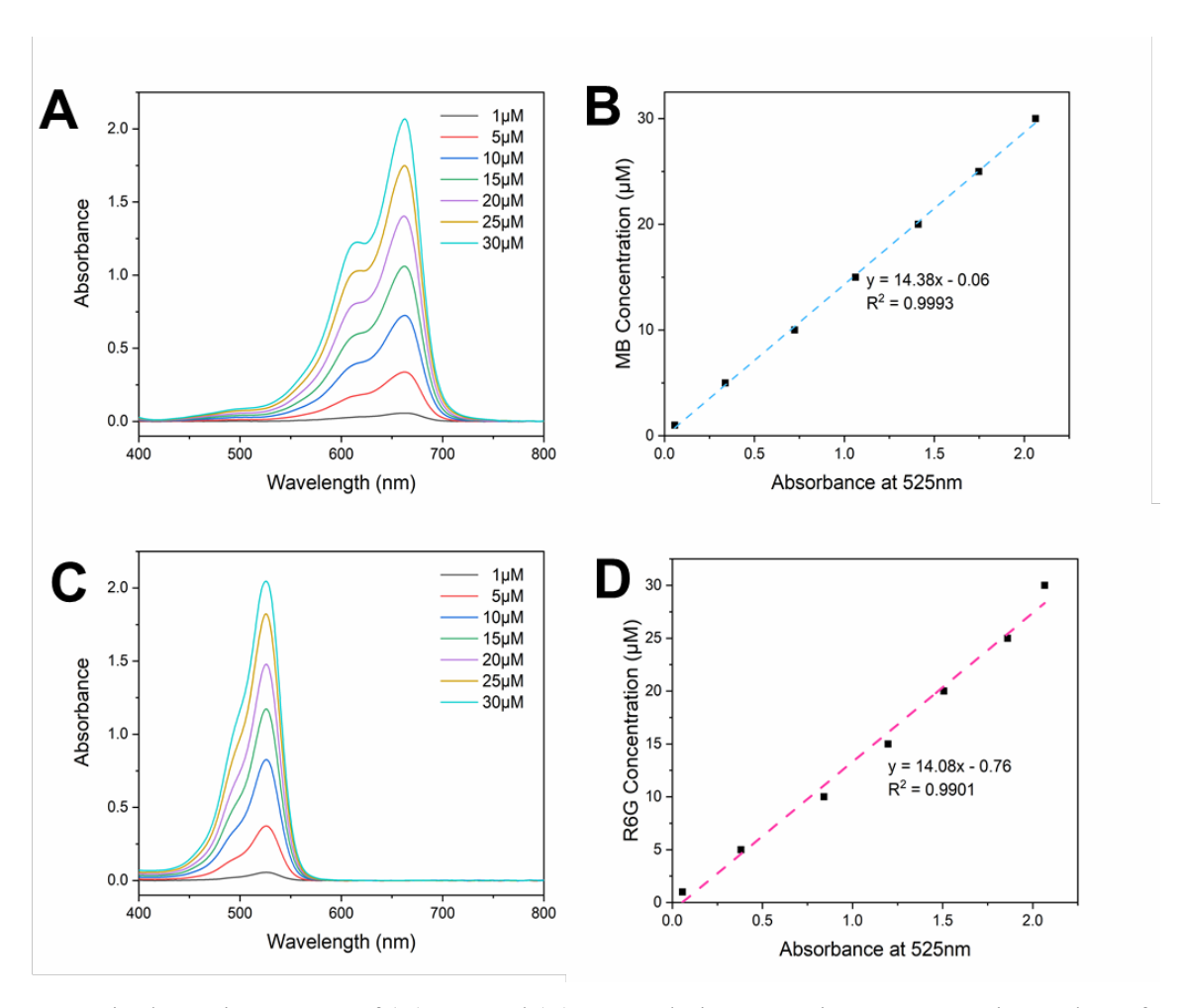


Figure S6. UV-vis absorption spectra of (A) MB and (C) R6G solutions at various concentrations. Plots of absorbance with respect to the concentrations of (B) MB and (D) R6G solutions at 660 nm and 525 nm, respectively.

S5.2 Dye absorption performance of 3D printed HKUST-1 hydrogel with different AAm concentrations

We examined the influence of the amount of AAm in the hydrogel matrix to the absorption performance of the HKUST-1 hydrogel, by recording the time-dependent MB adsorption of HKUST-1 hydrogel with 0.9, 1.8, 3.6 M AAm. The result (Fig. S7) suggest that the AAm concentration in the matrix doesn't impact the terminal removal rate, indicating that these hydrogels have very similar MOF loading rates. The time required to reach the terminal absorption decreases with increasing AAm concentration. We attribute this trend to the hydrophilicity of the composite which increases with increasing amount of the hydrophilic AAm in the matrix, resulting in a faster water update from the dye solution.

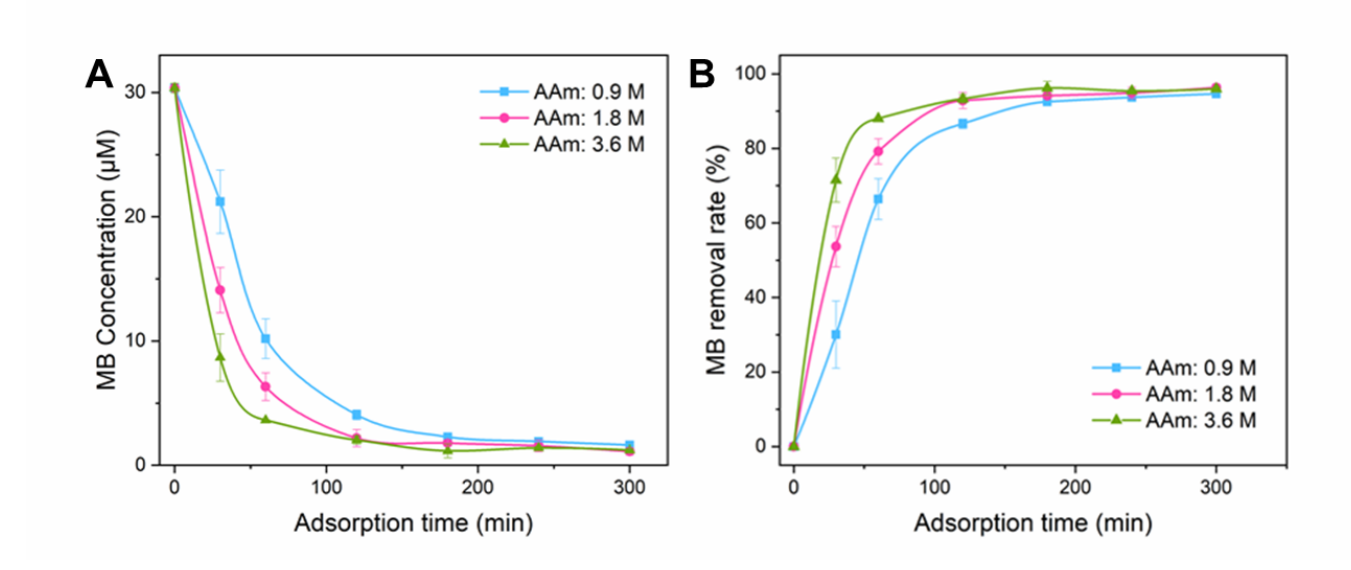


Figure S7. Dye absorption performance of HKUST-1 hydrogels with different AAm concentration. Plots of time-dependent, (A) dye concentration, and (B) dye removal rate of MB by 3D printed HKUST-1 hydrogel with different AAm concentrations.

References

- (1) McKellar, S. C.; Graham, A. J.; Allan, D. R.; Mohideen, M. I. H.; Morris, R. E.; Moggach, S. A. The Effect of Pressure on the Post-Synthetic Modification of a Nanoporous Metal-Organic Framework. *Nanoscale* **2014**, *6*, 4163–4173.
- (2) Lim, G. J. H.; Wu, Y.; Shah, B. B.; Koh, J. J.; Liu, C. K.; Zhao, D.; Cheetham, A. K.; Wang, J.; Ding, J. 3D-Printing of Pure Metal-Organic Framework Monoliths. *ACS Mater. Lett.* **2019**, *1*, 147–153.
- (3) Shi, Z.; Xu, C.; Chen, F.; Wang, Y.; Li, L.; Meng, Q.; Zhang, R. Renewable Metal-Organic-Frameworks-Coated 3D Printing Film for Removal of Malachite Green. *RSC Adv.* **2017**, *7*, 49947–49952.
- (4) Chowdhury, P.; Bikkina, C.; Meister, D.; Dreisbach, F.; Gumma, S. Comparison of Adsorption Isotherms on Cu-BTC Metal Organic Frameworks Synthesized from Different Routes. *Microporous Mesoporous Mater.* **2009**, *117*, 406–413.
- (5) Sun, J. Y.; Zhao, X.; Illeperuma, W. R. K.; Chaudhuri, O.; Oh, K. H.; Mooney, D. J.; Vlassak, J. J.; Suo, Z. Highly Stretchable and Tough Hydrogels. *Nature* **2012**, *489*, 133–136.